



**Magnetic order and strongly correlated effects in the one-dimensional Ising-Kondo lattice**Xiaofan Zhou , Jingtao Fan ,\* and Suotang Jia*State Key Laboratory of Quantum Optics and Quantum Optics Devices, Institute of Laser Spectroscopy,  
Shanxi University, Taiyuan 030006, China**and Collaborative Innovation Center of Extreme Optics, Shanxi University, Taiyuan 030006, China*

(Received 5 January 2024; revised 22 April 2024; accepted 23 April 2024; published 3 May 2024)

We investigate the magnetic order and related strongly correlated effects in a one-dimensional Ising-Kondo lattice with transverse field. This model is the anisotropic limit of the conventional isotropic Kondo lattice model, in the sense that the itinerant electrons interact with the localized magnetic moments via only longitudinal Kondo exchange. Adopting the numerical density-matrix renormalization group method, we map out the ground-state phase diagram in various parameter spaces. Depending on the Kondo coupling and filling number, three distinct phases, including a metallic paramagnetic, a metallic ferromagnetic, and a gapped spin-density wave phase, are obtained. The spin-density wave is characterized by an ordering wave vector, which coincides with the nesting wave vector of the Fermi surface. This makes the corresponding magnetic transition a spin analog of the Peierls transition occurring in the one-dimensional metal. Moreover, by analyzing the momentum distribution function and charge correlation function, the conduction electrons are shown to behave like free spinless fermions in the ferromagnetic phase. We finally discuss the effect of the repulsive Hubbard interaction between conduction electrons. Our paper enriches the Kondo physics and deepens the current understanding of the heavy fermion compounds.

DOI: [10.1103/PhysRevB.109.195112](https://doi.org/10.1103/PhysRevB.109.195112)**I. INTRODUCTION**

As one of the most important canonical models in condensed matter systems, the Kondo lattice model (KLM) is used to describe the process where a conduction band, occupied by itinerant fermions, interacting with a lattice of localized magnetic moments [1]. The KLM is relevant to a wide class of real materials called heavy fermion system [2–11], in which huge quasiparticle mass can emerge due to the formation of Kondo singlets [12,13]. The study of such heavy fermion materials is believed to be critical for understanding diverse phenomena such as quantum criticality [5,14–20] and high- $T_c$  superconducting compounds [2–4]. While the well-solved single-impurity Kondo problem provides some useful concepts for the KLM, there are aspects where the single-impurity results have no analog in the lattice case [21–23]. For example, except for a few exact results in certain limits [24–26], the dynamical details of the interplay between the local Kondo physics and the nonlocal Ruderman-Kittel-Kasaya-Yosida (RKKY) interaction remains elusive. As a consensus that has been reached, under zero temperature, the one-dimensional (1D) KLM presents three distinct magnetic phases: the antiferromagnetic phase (AFM) with fully opened spin and charge gaps, the metallic paramagnetic phase (PM) with RKKY correlations, and the metallic ferromagnetic phase (FM) [3,27–32]. The AFM is stable down to zero Kondo coupling when the conduction band is half-filled, whereas the

PM-to-FM transition can occur only away from half filling [33–35].

The KLM respects a SU(2) rotational symmetry due to the isotropic Kondo interaction in the spin space. However, by adding anisotropy between the Kondo couplings, numerous interesting physics, which is beyond the isotropic model, can emerge [36–38]. For example, the KLM with properly tuned anisotropy has been utilized to understand the physics of the dissipative two-state systems [39,40]. Moreover, it has been shown that the ferromagnetic Kondo couplings with easy-plane anisotropy may yield anomalous singlet formation [41]. Among various kinds of anisotropy introduced in the KLM, the Ising-Kondo lattice model (IKL) with only longitudinal Kondo coupling takes on a special role [42–52]. Its importance is due both to its simple Ising-type coupling form, amenable to both analytical and numerical treatments [50], and to its relevance to a series of real materials [46–49]. The IKL was first proposed to describe the concurrence of large specific heat jump and weak antiferromagnetism in URu<sub>2</sub>Si<sub>2</sub> [46]. Recently, some thermodynamic properties of the IKL [50], including the antiferromagnetic topological character [51] and the emergent strange metal behaviors [52], were discussed on two-dimensional lattices. However, a systematic understanding of the magnetic order in the IKL under various conduction electron concentrations, especially for the 1D case, is still lacking.

In this paper, we investigate the ground-state properties of the 1D IKL with transverse field by using the numerical density-matrix renormalization group (DMRG) method [53,54]. The competition between the nonlocal RKKY mechanism and the local Kondo physics leads to the emergence

\*fanjt@sxu.edu.cn

of magnetic correlations and, consequently, various magnetic orders. Apart from the metallic PM and FM, a gapped spin-density wave phase (SDW) with long-range order is unraveled. The ordering wave vector characterizing the SDW is found to be nothing but the nesting wave vector of the Fermi surface constructed by the conduction electrons, making the SDW a Peierls-like insulator. We also discuss the effect of repulsive Hubbard interaction imposed on the magnetic orders. It is revealed that the Hubbard interaction influences the magnetic phases in a way much like the Kondo coupling; it can trigger both the PM-to-SDW and SDW-to-FM transitions, depending on the filling number of the conduction electrons.

## II. MODEL AND METHOD

The IKL in consideration can be described by the following Hamiltonian ( $\hbar = 1$  throughout):

$$\hat{H} = -t \sum_{\langle i,j \rangle, \sigma} \hat{c}_{i,\sigma}^\dagger \hat{c}_{j,\sigma} + J \sum_j \hat{s}_j^z \hat{S}_j^z + \Delta \sum_j \hat{S}_j^x + \frac{U}{2} \sum_j \hat{n}_{j,\uparrow} \hat{n}_{j,\downarrow}, \quad (1)$$

where  $\hat{c}_{i,\sigma}^\dagger$  ( $\hat{c}_{i,\sigma}$ ) is the creation (annihilation) field operator of the conduction electron with spin  $\sigma$  ( $=\uparrow, \downarrow$ ) at lattice site  $j$ . The conduction electrons can hop between adjacent sites  $\langle i, j \rangle$  with the hopping rate  $t$ .  $\hat{S}_j^z$  denotes the  $z$  component of the spin-1/2 operator for the localized magnetic moment. The spin operator  $\hat{S}_j^z$  for the conduction electrons is defined by  $\hat{S}_j^z = \sum_{\tau,\tau'} \hat{c}_{j,\tau}^\dagger \sigma_{\tau,\tau'}^z \hat{c}_{j,\tau} / 2$  where  $\sigma^z$  is the Pauli- $z$  matrix. With these definitions, the second term of Hamiltonian (1) denotes the longitudinal Kondo interaction between the conduction electron and the localized moment at the same site  $j$ . The interaction strength  $J$  is assumed to be positive, implying an antiferromagnetic Kondo coupling. Note that for the IKL considered here, the ferromagnetic coupling with  $J < 0$  is connected to the antiferromagnetic case through a simple spin rotation, which is in contrast to the conventional isotropic KLM. The latter can exhibit dramatic different Kondo physics depending on the sign of the coupling strength [55,56]. A transverse field  $\Delta$ , introducing additional nonadiabaticity, is applied on the localized moments [46]. The direct repulsive interaction between conduction electrons is also included through the last Hubbard- $U$  term. In this paper, our main focus will be on the ground-state properties of the conduction electrons. The local moments construct the same magnetism with conduction electrons due to the longitudinal Kondo coupling term  $\sim \hat{s}_j^z \hat{S}_j^z$ . In the following discussion, we set the energy scale by taking  $t = 1$ , and we also take  $\Delta = 1$  unless otherwise specified.

The Hamiltonian (1), with vanishing transverse Kondo couplings (i.e.,  $\hat{s}_j^x \hat{S}_j^x + \text{H.c.} \rightarrow 0$ ), represents essentially the anisotropic limit of the conventional KLM [1]. In the adiabatic limit with  $\Delta = 0$ , the IKL is exactly solvable since the localized moment at each site is conservative obeying  $[\hat{S}_j^z, \hat{H}] = 0$ . The thermodynamic properties of the IKL under this condition has been preliminarily touched by Monte Carlo simulations [50]. A nonzero transverse field  $\Delta$ , however, breaks the conservativeness of  $\hat{S}_j^z$  and adds quantum

fluctuations to the localized moments. In this sense, the localized moments in the IKL can be alternatively viewed as lattice degrees of freedom, which impose dynamic potentials on the conduction electrons. The interactions between fermions and lattice degrees of freedom become specially important in 1D due to the perfect Fermi surface nesting [57,58]. One of the most noted consequences, for example, is the Peierls transition, characterized by the formation of a charge-density wave ordered at the nesting wave vector [59]. In light of the Ising-type interaction between conduction electrons and localized moments, in the IKL, we expect that an analogous SDW instability of the conduction electrons can be reached through similar mechanisms. This point will be further elucidated in the subsequent sections.

The magnetic order of the conduction electrons can be effectively characterized by the spin structure factor,

$$S(k) = \frac{1}{L} \sum_{l,j} \langle \hat{s}_l^z \hat{s}_j^z \rangle e^{i(l-j)k}, \quad (2)$$

where  $L$  is the number of lattice sites and  $\langle \dots \rangle$  denotes the ground-state average. The peak position in  $S(k)$ , denoted by an ordering wave vector  $k^{\text{max}}$ , characterizes the spatial variation of spin orientations projected into the  $z$  direction. Alternatively, we can characterize the magnetic order using the spin correlation function in real space

$$s(r) = \frac{1}{L} \sum_l \langle \hat{s}_l^z \hat{s}_{l+r}^z \rangle, \quad (3)$$

where  $r$  is the distance between different sites. The correlation function  $s(r)$  has the advantage of intuitively showing the spatial distribution of the spin correlations. The equivalence between  $S(k)$  and  $s(r)$  can be clearly found by noting that they constitute a Fourier transform pair. In the spirit of Landau's paradigm, the magnetic ordering is characterized by spontaneously broken symmetry at some ordering wave vector  $k^{\text{max}}$ . This implies the existence of long-range order, which can be identified by scaling the spin structure factor [60],

$$\lim_{L \rightarrow \infty} \frac{1}{L} S(k^{\text{max}}) > 0. \quad (4)$$

The long-range nature is also manifested in the correlation function  $s(r)$  by  $\lim_{r \rightarrow \infty} s(r) \neq 0$ . Therefore, we can identify different magnetic phases according to Eq. (4) by extrapolating the spin structure factor to the thermodynamic limit  $L \rightarrow \infty$ . In this way, we may obtain the  $k^{\text{max}}$ -ordered SDW for  $k^{\text{max}} \neq 0$  and the FM for  $k^{\text{max}} = 0$ . If  $S(k)/L$  is extrapolated to be zero in the thermodynamic limit, the corresponding phase loses any magnetic long-range order and is thus termed PM. We emphasize that, due to the space-inversion symmetry of the system, any peaks in  $S(k)$ , if exist, should be exactly symmetric about  $k = 0$ .

Here, we perform state-of-the-art DMRG calculations to compute the many-body ground state of the system, with which various physical observable can be obtained. In our numerical simulations, the filling number  $\rho = N/L$  is a good quantum number, which can be varied from zero to one. Here  $N$  is the total number of conduction electrons. We set lattice size up to  $L = 60$ , and work with open boundary conditions. For each lattice size, we retain 600 truncated states per DMRG

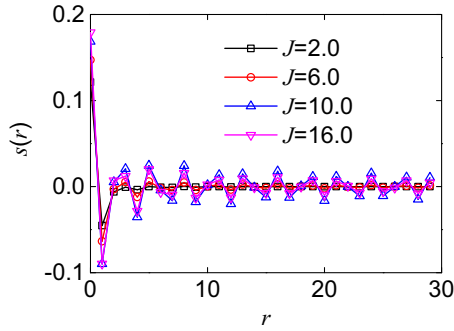


FIG. 1. The correlation function  $s(r)$  for systems with  $\rho = 0.75$ ,  $L = 60$ , and a varying  $J$ .

block and perform 20 sweeps with a maximum truncation error of  $\sim 10^{-9}$ .

### III. MAGNETIC CORRELATIONS INDUCED BY KONDO COUPLING

We first clarify the effect of the Kondo coupling  $J$  by setting  $U = 0$ . Before showing the numerical results, some qualitative insights can be gained by inspecting different parameter regimes. For the coupling strength comparable with or less than the Fermi energy of the conduction electrons, the dominant ordering force turns out to be the RKKY correlation with Ising anisotropy, which compete with the quantum fluctuations induced by the transverse field  $\Delta$ . Increasing  $J$  further to the intermediate coupling regime, the disorder created by  $\Delta$  is irrelevant and the interplay between the RKKY-type interactions and the local Kondo physics becomes important. At extremely strong coupling  $J \gg 1$ , the conduction electrons and the local moments are tightly bound together to form antiferromagnetic Ising pairs (AIPs). Similar to the Kondo singlet formed in the isotropic KLM, the AIPs here are site localized and may give rise to distinct local Kondo physics [61]. We thus expect rich long-range magnetic orders may emerge throughout the whole range of the coupling strength.

#### A. Phase transitions and long-range order

Let us discuss in detail the magnetic phase behaviors of the IKL in different coupling regimes. Figure 1 shows the correlation function  $s(r)$  with  $\rho = 0.75$  and different  $J$ . When  $J$  is relatively weak, the spin correlation rapidly decays to zero as the distance  $r$  increases. For larger  $J$ , we observe a persistent oscillation of  $s(r)$  instead. This nondecaying behavior of spin correlation signals the emergence of a long-range magnetic order.

The transitions between different magnetic phases becomes clearer if we investigate the corresponding spin structure factor  $S(k)$ . The left column of Fig. 2(a1)–2(c1) plot  $S(k)/L$  for three different values of  $J$  with  $\rho = 0.75$ . The results for different system sizes are labeled by lines with different colors. The values of  $L \rightarrow \infty$  are obtained by the standard finite-size scaling. The right column of Fig. 2(a2)–2(c2) demonstrate the scaling details for three characteristic wave vectors. We first focus on the weak coupling strength with  $J = 2.0$  [Fig. 2(a1)]. It is shown that  $S(k)/L$  develops

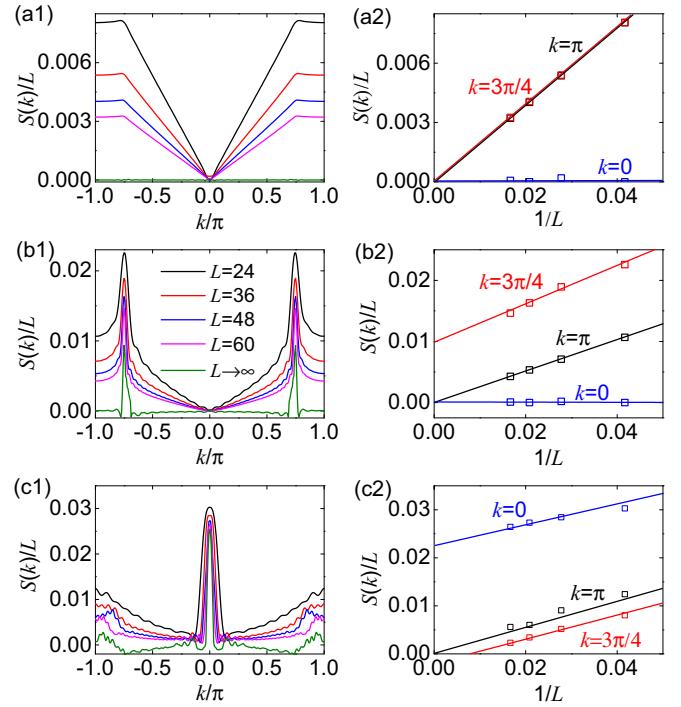


FIG. 2. (a1)–(c1) The scaled spin structure factor  $S(k)/L$  and (a2)–(c2) the corresponding finite-size scalings at three characteristic wave vectors for systems with (a)  $J = 2.0$ , (b)  $J = 10.0$ , and (c)  $J = 22.0$ . Different system sizes are characterized by lines with different colors. In these figures, we set  $\rho = 0.75$  and  $U = 0$ .

weak peaks at  $k = k^{\max} = \pm 2k_F$  for any finite-system sizes, resulting from a RKKY-type correlation. Here  $k_F = \pi\rho/2$  is the Fermi momentum of the conduction electron. As the system size increases, however, the peaks become weaker and weaker and eventually disappear in the thermodynamic limit  $L \rightarrow \infty$ . This implies that the magnetic correlations built up in this regime is essentially short range, and consequently give rise to the appearance of PM. Something interesting happens if the coupling strength increases. The spin structure factor with  $J = 10.0$  is shown in Fig. 2(b1). It is found that, while the structure with  $k^{\max} = \pm 2k_F$  still exists, the peaks become much higher and sharper compared to  $J = 2.0$ . Accordingly, the scaled structure factor  $S(k = k^{\max})/L$  is extrapolated to a finite value in the thermodynamic limit [see the red line in Fig. 2(b2)], indicating the existence of a SDW, which is ordered at  $k = k^{\max}$ . This is in sharp contrast with the isotropic KLM. In that case, the conduction electrons lose the true SDW order due to additional fluctuations, although short-range magnetic correlations still exist [3]. Increasing  $J$  further, the conduction electrons and localized moments start to be bound together and the tendency of local AIP formation overwhelms that of the RKKY-type correlation. As a result, a sharp peak at  $k = 0$  grows up whereas density waves at other wave vectors are greatly suppressed, as shown in Fig. 2(c1). This structure of  $S(k)$  unambiguously demonstrates the ferromagnetism. We thus find that as  $J$  increases, the system starts from PM, and subsequently traverses the SDW, and eventually evolves to the FM.

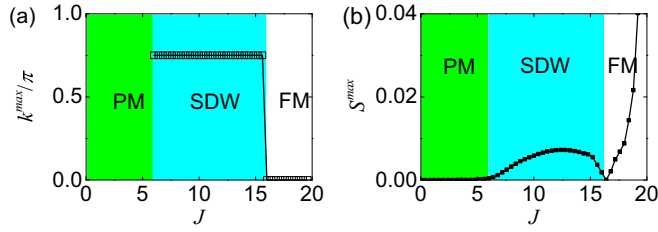


FIG. 3. (a) The ordering wave vector  $k^{\max}$  and (b) the ordering strength  $S^{\max}$  as functions of  $J$  with  $\rho = 0.75$  and  $U = 0$ .

To provide a more precise picture, we monitor the ordering wave vector  $k^{\max}$  as a function of the coupling strength for  $\rho = 0.75$ . Considering the inherent inversion symmetry of  $S(k)$  about  $k = 0$ , we here focus on the  $k^{\max} \geq 0$  part. As shown in Fig. 3(a),  $k^{\max}$  is not well defined for  $J < 5.8$  due to the general vanishing of  $S(k)/L$  in the limit of  $L \rightarrow \infty$ , which is the character of the PM. Increasing  $J$  above 5.8, a well-defined  $k^{\max}$  emerges at  $2k_F$ , and keeps at that value until it drops to zero where the FM is formed. The feature that  $k^{\max}$  keeps constant before reaching FM is different from the isotropic KLM, where the peaks in  $S(k)$  can move continuously toward zero as  $J$  increases [56]. Figure 3(b) plots  $S^{\max}$ , which we dub ordering strength, in terms of  $J$ .  $S^{\max}$  is the maximum of the scaled spin structure factor  $\lim_{L \rightarrow \infty} S(k)/L$  within the Brillouin zone. With this definition, we find the relation  $S^{\max} = \lim_{L \rightarrow \infty} S(k^{\max})/L$  applies in the ordered phase. It follows that  $S^{\max}$ , together with the value of  $k^{\max}$ , serve as complete order parameters characterizing the ordering process of different magnetic phases. As shown in Fig. 3(b), while  $S^{\max}$  remains zero in the PM, it gradually increases from zero, reaching the maximum, and then decreases until vanishes at the critical point  $J_c = 16.4$ . Above  $J_c$ , the system enters the FM with monotonically increased  $S^{\max}$ .

The nonmonotonical behavior of  $S^{\max}$  results from the competition between the RKKY-type interaction and the AIP formation. The details of this competition is partially manifested in the correlation function between the conduction electron and local moment,

$$S_{\text{cf}}(r) = \frac{1}{L} \sum_l \langle \hat{s}_l^z S_{l+r}^z \rangle. \quad (5)$$

As defined in Eq. (5), the correlation function  $S_{\text{cf}}(r)$  measures the nonlocal character of the antiferromagnetic Ising bond between the conduction electrons and local moments [28]. Figure 4(a) plots  $S_{\text{cf}}(r)$  with a varying values of  $J$ . At weak coupling  $J = 2$ , the hybridization between the conduction electron and local moment is ineffective, yielding a rather weak signal in  $S_{\text{cf}}(r)$ . For larger  $J$ ,  $S_{\text{cf}}(r)$  increases in height and it decays very slowly as  $r$  increases, reflecting a sizable extension of the Ising bond. This long-range behavior of  $S_{\text{cf}}(r)$  signals the appearance of a regime where the RKKY mechanism may work. Increasing the coupling strength further such that  $J \gtrsim 12$ ,  $S_{\text{cf}}(r)$  becomes more and more localized, implying that the size of the Ising bond reduces, and the RKKY mechanism is suppressed. This point is further strengthened by examining the on-site correlation  $S_{\text{cf}}(0)$  versus  $J$ . As shown

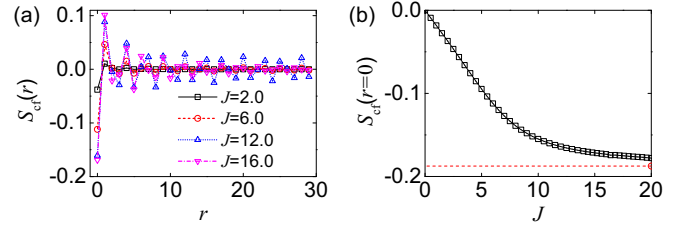


FIG. 4. (a) The correlation function  $S_{\text{cf}}(r)$  for different  $J$ . (b) The on-site value  $S_{\text{cf}}(0)$  as a function  $J$ . The other parameters in these figures are  $\rho = 0.75$ ,  $U = 0$ , and  $L = 60$ . The red-dashed line in (b) denotes the value of the perfect AIPs.

in Fig. 4(b), as  $J$  increases,  $S_{\text{cf}}(0)$  approaches asymptotically that of perfect AIPs  $-\rho/4$  (the red-dashed line).

Up to now, our discussion is limited to a specific band filling of the conduction electrons, namely  $\rho = 0.75$ . We have observed that the ordering wave vector of the SDW in this filling is fixed by the Fermi momentum of the conduction electrons via  $k^{\max} = \pm 2k_F$ . In fact, this relation applies to any fillings provided the system is within the SDW. To demonstrate this, we plot  $k^{\max}$  and  $S^{\max}$  as functions of  $\rho$  with  $J = 12.0$  in Figs. 5(a) and 5(b), respectively. As an immediate finding, while  $k^{\max}$  keeps filling independent in the FM and PM, it follows  $\rho$  linearly through  $k^{\max} = \pm 2k_F$  in the SDW region [see Fig 5(a)]. Notice that the ordering wave vector  $2k_F$  is exactly the nesting wave vector of the Fermi surface, which characterizes the charge-density wave in an Peierls insulator [59]. It is thus inferred that the appearance of the SDW in the 1D IKL can be traced back to the perfect Fermi surface nesting effect. The latter drastically modifies the band structure of itinerant electrons. From this point of view, the formation of SDW in the IKL can be regarded as a magnetic analog of the Peierls transition, which occurs in the charge degree of freedom.

## B. Phase diagram

With the understanding above, we map out the phase diagram in the  $J - \rho$  plane in Fig. 6. As can be seen, the PM occupies most portion of the phase diagram for weak coupling strength, due to the dominant quantum fluctuations of the local moments. As  $J$  increases, the ordered phases, including FM and SDW with various ordering wave vectors, emerge. Whereas the SDW is more favored when the filling number is closed to  $\rho = 1$ , the FM is formed away from this half-filling case. The ordering process for  $J = 12.0$  is

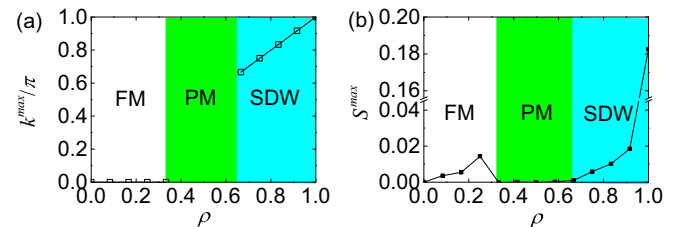


FIG. 5. (a) The ordering wave vector  $k^{\max}$  and (b) the ordering strength  $S^{\max}$  as functions of  $\rho$  with  $J = 12.0$  and  $U = 0$ .

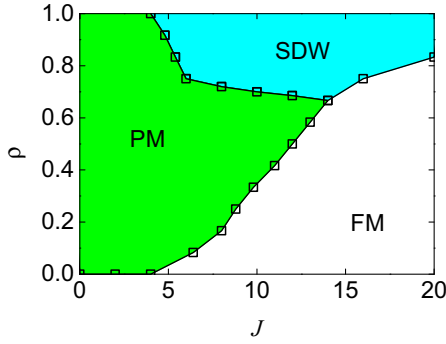


FIG. 6. The phase diagram in the  $J - \rho$  plane with  $U = 0$ . The phase boundaries have been extrapolated to the thermodynamic limit  $L \rightarrow \infty$ .

illustrated in Fig. 5(b), where we find  $S^{\max}$  increases rapidly as  $\rho$  approaches one. We emphasize that the SDW for  $\rho = 1$  is an antiferromagnetic insulator characterized by a Néel configuration with finite spin and charge gaps [50]. Increasing  $J$  above 14.0, the PM generally disappears and the SDW region starts to shrink. The antiferromagnetic insulator for  $\rho = 1$ , however, remains stable against the ferromagnetization even in the  $J \rightarrow \infty$  limit [50].

The mechanism of different magnetic structures closed to and far away from half filling can be understood as follows. As illustrated in Fig. 7(a), in the strong coupling regime and around half-filling, each neighbor sites of the conduction electron is likely to be occupied by another one, since double occupancy of the conduction electrons on the same site would elevate the energy by  $\Delta E \sim J/4$ . As a result, the hopping between neighbor sites is forbidden by the Pauli exclusion principle if the spins of conduction electrons align in the same direction. However, if the spins form an antiferromagnetic configuration, a virtual tunneling process can occur, which lowers the kinetic energy of the conduction electrons by  $\Delta E \sim 4t^2/J$ , resembling closely the superexchange process in the Hubbard model [60]. Far away from half filling, on the other hand, the conduction electrons can freely move along the lattice without costing any additional energy once their spins are aligned parallel to each other [see Fig. 7(b)].

The above picture hints that the system is a gapped insulator throughout the SDW (not only the half-filling case) and becomes metallic when moving into FM and PM. This proposition is corroborated by calculating the scaling of the entanglement entropy between a block of size  $l$  and the rest of the system,  $S_l = -\text{Tr}(\rho_l \ln \rho_l)$ , where  $\rho_l = \text{Tr}_{L-l}|\Psi\rangle\langle\Psi|$  is the reduced density matrix corresponding to the block. For 1D systems, gapped phases follows an area law, and the

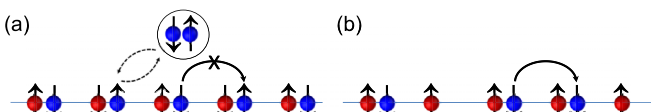


FIG. 7. Schematic illustration of the magnetic structures when the conduction electrons are (a) around and (b) far away from half filling. In these figures, the red and blue balls denote the localized moments and conduction electrons, respectively.

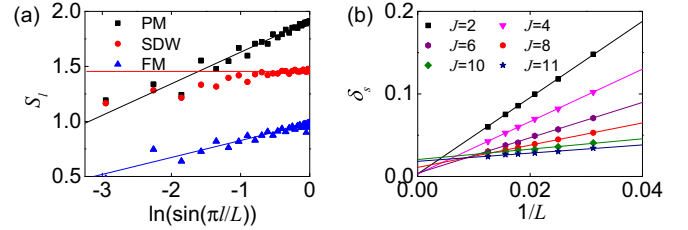


FIG. 8. (a) The entanglement entropy  $S_l$  in terms of the block size  $l$ , for representative points of PM ( $J = 2.0$ ,  $\rho = 0.75$ ), SDW ( $J = 8.0$ ,  $\rho = 0.75$ ), and FM ( $J = 18.0$ ,  $\rho = 0.5$ ) with  $L = 60$ . The scaling behavior for different phases are plotted by lines with different colors. (b) The finite-size scaling of spin gap  $\delta_s$  for  $\rho = 0.75$  and different  $J$ . In these figures, we fix the Hubbard interaction as  $U = 0.0$ .

entanglement entropy  $S_l$  would saturate as  $l$  increases [62].  $S_l$  in gapless phases, however, does not saturate but grows logarithmically when increasing  $l$  [63]. The scaling of  $S_l$  for three representative points in the phase diagram are shown in Fig. 8(a). While the presence of a gap in the SDW is indicated by the saturation of  $S_l$ , the FM and PM are both gapless since  $S_l$  logarithmically diverges with the block's size.

To better understand the gapped nature of the SDW, it is instructive to compute spin gap directly in this phase. Given that the global net magnetization of conduction electrons is zero for both PM and SDW, the spin gap can be conveniently defined for these states as

$$\delta_s = E_g(s_{\text{tot}}^z = 1) - E_g(s_{\text{tot}}^z = 0), \quad (6)$$

where  $E_g(s_{\text{tot}}^z)$  is the ground-state energy with invariant total spin  $s_{\text{tot}}^z$  of the conduction electrons. Figure 8(b) plots the spin gaps  $\delta_s$  as a function of  $1/L$  for  $\rho = 0.75$  and various  $J$ . For relatively small  $J$ ,  $\delta_s$  extrapolates nicely to zero as  $L \rightarrow \infty$ , indicative of a gapless state. However, for larger coupling strength ( $J > 6$ ) at which the SDW is reached, the spin gap  $\delta_s$  extrapolates to a finite value as  $L \rightarrow \infty$ . We emphasize that such a nonzero spin gap was found throughout the SDW, indicating the stability of this state against spin fluctuations.

### C. Momentum distribution of the conduction electrons

The interplay of the localized and itinerant behaviors in the IKL can be alternatively characterized by the momentum distribution function of the conduction electrons,

$$n(k) = \frac{1}{L} \sum_{l,j} \langle \hat{c}_{l\sigma}^\dagger \hat{c}_{j\sigma} \rangle e^{i(l-j)k}. \quad (7)$$

Figure 9(a) shows the variation of  $n(k)$  with increasing  $J$  for  $\rho = 0.5$ . For small  $J$ , as expected, the Fermi surfaces of the conduction electrons is clearly formed at  $k_F = \pm\pi\rho/2$ . As  $J$  increases, the conduction electrons start to be hybridized with the local moments, which broadens the distribution of  $n(k)$  and blurs the original Fermi surfaces. For even larger  $J$ , two sharp edges in  $n(k)$ , separating the occupied and unoccupied states, appear at  $k_F^L = 2k_F = \pm\pi\rho$ . Further increasing  $J$  has little effect on the structure of  $n(k)$ , indicating that the system has reached a strong coupling regime with a well-defined large Fermi surface. The variations in the structure of  $n(k)$  is

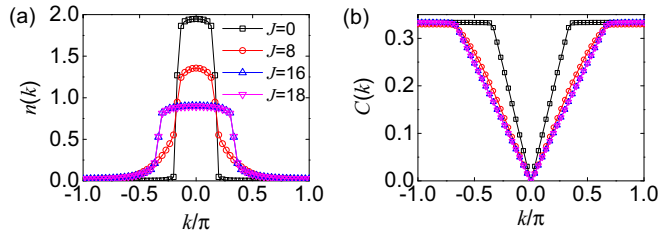


FIG. 9. (a) The momentum distribution function  $n(k)$  and (b) the charge structure factor  $C(k)$  for systems with  $\rho = 1/3$ ,  $U = 0$ ,  $L = 60$  and a varying  $J$ .

accompanied by corresponding changes in the charge structure factor, defined by

$$C(k) = \frac{1}{L} \sum_{l,j} (\langle \hat{n}_l \hat{n}_j \rangle - \langle \hat{n}_l \rangle \langle \hat{n}_j \rangle) e^{i(l-j)k}. \quad (8)$$

As shown in Fig. 9(b), we plot  $C(k)$  for the same values of  $J$  as those used in Fig. 9(a). When  $J$  is small,  $C(k)$  exhibits two cusps at  $k_c = \pm\pi\rho$ , manifesting the free particle nature of the conduction electrons. The cusps, however, is smoothed at intermediate values of  $J$ , exhibiting characters of strongly interacting fermions. Moving into the strong coupling regime with larger  $J$ , two new cusps are formed at  $k_c^L = \pm 2\pi\rho$ . Through a careful analysis of  $n(k)$  and  $C(k)$  for different filling numbers, we find that the appearances of the characteristic wave vectors  $k_F^L$  and  $k_c^L$  are always accompanied by the formation of FM. The above signatures of  $n(k)$  and  $C(k)$  strongly suggest that, in the strong coupling regime, the conduction electrons behave like free spinless fermions.

To understand this, let us start from a half-filled IKL with  $N (= L)$  conduction electrons. In the strong coupling regime, each local moment tend to catch an electron to form an AIP, ending up with a 1D liquid composed of  $L$  AIPs. Doping away from half filling amounts to adding holes to the system. Note that double occupancy of holes on the same lattice site is naturally excluded by definition. As discussed above, when the spins of conduction electrons are aligned parallel to each other, the system can lower its energy by allowing the holes freely moving on the lattice. Otherwise the hopping process of holes may elevate energy due to the strong Kondo coupling. Suppose now we have  $L - N$  holes ( $N < L$ ) moving in the sea of the AIP background. The Fermi momentum of these mobile holes is thus  $k_F^h = [1 - (L - N)/L]\pi = \rho\pi = k_F^L$ , exactly at the large Fermi surface.

#### IV. EFFECT OF THE REPULSIVE HUBBARD INTERACTION

We proceed to discuss the effect of finite repulsive Hubbard interaction  $U$ . Following the same manner used in Sec. III, we present the phase diagram in the  $J - U$  plane for  $\rho = 0.75$  in Fig. 10(a). One of the direct impacts of the Hubbard interaction is that the FM becomes more robust. As  $U$  increases, the phase boundary between FM and SDW is persistently pushed to lower value of  $J$ , until  $U \approx 60$ , for which the SDW disappears and the FM directly touches the PM. The stabilization of FM by  $U$  is also predicted in the isotropic KLM [8,26] and can

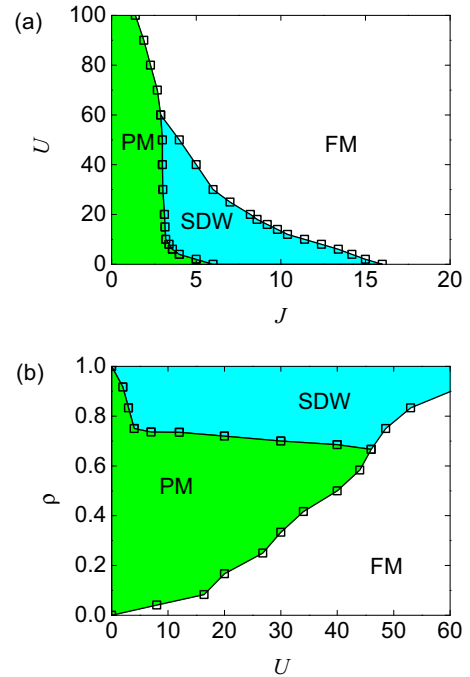


FIG. 10. (a) The phase diagram in the  $J - U$  plane with  $\rho = 0.75$  and (b) the phase diagram in the  $\rho - U$  plane with  $J = 4.0$ . The phase boundaries in (a) and (b) have been extrapolated to the thermodynamic limit  $L \rightarrow \infty$ .

be understood on physical grounds; the repulsive interaction enhances the energy penalty costed by double occupancy of the conduction electrons on the same lattice site, which promotes the formation of the on-site AIP. The latter becomes mobile if the lattice is doped far away from half filling, and thus favors ferromagnetism through the Kondo mechanism we mentioned at the last of Sec. III. It is interesting to find that the critical value of  $J$  at which PM-to-SDW transition occurs presents great dependence on the Hubbard interaction when  $U$  is relatively small. As the Hubbard interaction increases, however, this critical value appears to saturate at  $J_c \approx 3.0$ , showing no explicit dependence on  $U$ . The saturation value of  $J_c$  terminates at  $U \approx 60$ , above which the SDW disappears.

To see clearly the role of  $U$  in inducing various phase transitions, we plot  $k^{\max}$  and  $S^{\max}$  as functions of  $U$  for two different values of  $J$  in Fig. 11. It is to be seen that, depending on the value of  $J$ , the repulsive interaction can drive various magnetic phase transitions, including PM-to-SDW, SDW-to-FM [Figs. 11(a1) and 11(a2)], and PM-to-FM [Figs. 11(b1) and 11(b2)] transitions. We find again that the ordering wave vector  $k^{\max}$  in the SDW is independent of  $U$  and uniquely specified by the Fermi momentum. As such, the phase transition driven by  $U$  is of course filling dependent. The general result is summarized in the  $\rho - U$  phase diagram for  $J = 4.0$  [see Fig. 10(b)]. We observe that the filling number influences the phase transitions in a similar fashion as that in the  $J - \rho$  phase diagram (see Fig. 6); the transition from PM to FM turns out to be easier for low electron filling, and the SDW is stabilized only closed to half filling.

Along the logic in Sec. III, let us examine the impact of  $U$  on the momentum distribution function and charge structure

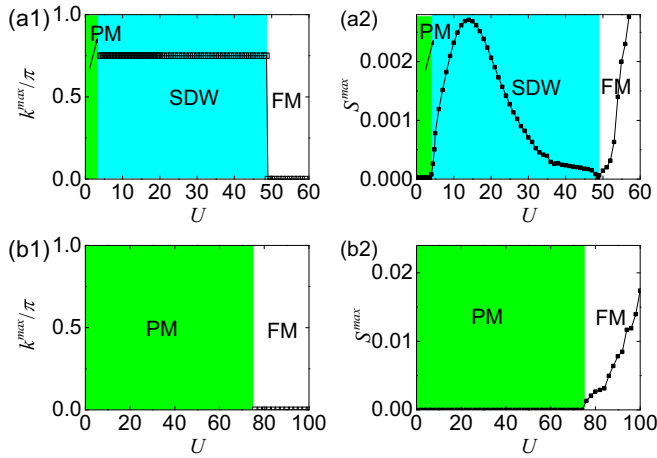


FIG. 11. (a1)-(b1) The ordering wave vector  $k^{\max}$  and (a2)-(b2) the ordering strength  $S^{\max}$  as functions of  $U$  for systems with (a)  $J = 4.0$  and (b)  $J = 2.5$ . In these figures, we set  $\rho = 0.75$ .

factor. The variations of  $n(k)$  and  $C(k)$  with  $\rho = 0.5$  and  $J = 4.0$  and a varying values of  $U$  are respectively shown in Figs. 12(a) and 12(b). As depicted in these figures, when increasing  $U$ , both  $n(k)$  and  $C(k)$  exhibit the same behaviors as those shown in Fig. 9. Especially when  $U$  is sufficiently large for which the FM is reached, the aforementioned large Fermi surface is clearly formed at  $k_F^L = \pm\pi\rho$ , suggesting a ferromagnetic metal.

As can be found from above discussion, the role of repulsive Hubbard interaction presents great similarities with the Kondo coupling  $J$ , hinting that it may work through renormalizing  $J$ . The full clarification of the connection between  $U$  and  $J$  in the IKL may require some more sophisticated analytical approaches, such as renormalization group and bosonization, which is out of the scope of the present paper and merits a separate study in the future.

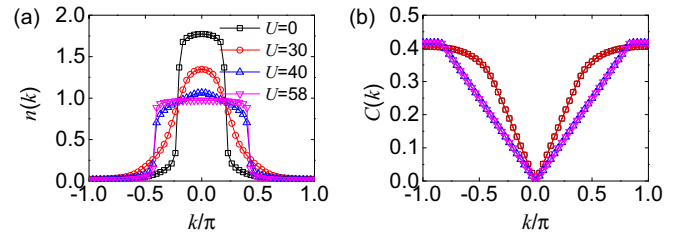


FIG. 12. (a) The momentum distribution function  $n(k)$  and (b) the charge structure factor  $C(k)$  for systems with  $\rho = 0.42$ ,  $J = 4.0$ ,  $L = 60$ , and a varying  $U$ .

## V. CONCLUSIONS

In conclusion, we have studied the ground-state properties of the 1D IKL by using the numerical density-matrix renormalization group (DMRG) method. Three distinct quantum phases, including a metallic PM, a metallic FM, and a gapped SDW, have been obtained. The SDW is characterized by an ordering wave vector, which coincides with the nesting wave vector of the Fermi surface. This makes the PM-to-SDW transition a magnetic analog of the Peierls transition, which occurs in the charge degree of freedom of a one-dimensional metal. Moreover, by analyzing the momentum distribution function and charge correlation function, the conduction electrons are shown to behave like free spinless fermions in the FM. The effect of the repulsive Hubbard interaction between conduction electrons has also been clarified.

## ACKNOWLEDGMENTS

This work is supported by the National Key Research and Development Program of China under Grant No. 2022YFA1404003, the National Natural Science Foundation of China (NSFC) under Grant No. 12174233, 12004230 and 12034012, the Research Project Supported by Shanxi Scholarship Council of China and Shanxi '1331KSC'. Our simulations make use of the ALPSCore library [64], based on the original ALPS project [65].

- [1] S. Doniach, The Kondo lattice and weak antiferromagnetism, *Phys. B: Condens. Matter* **91**, 231 (1977).
- [2] A. C. Hewson, *The Kondo Problem to Heavy Fermions* (Cambridge University Press, Cambridge, 1993).
- [3] H. Tsunetsugu, M. Sigrist, and K. Ueda, The ground-state phase diagram of the one-dimensional Kondo lattice model, *Rev. Mod. Phys.* **69**, 809 (1997).
- [4] E. Huecker and Y. Komijani, Spin fractionalization in a Kondo-lattice superconductor heterostructure, *Phys. Rev. B* **108**, 195120 (2023).
- [5] Q. Si, J. L. Smith, and K. Ingersent, Quantum critical behavior in Kondo systems, *Int. J. Mod. Phys. B* **13**, 2331 (1999).
- [6] P. Coleman, C. Pépin, Q. Si, and R. Ramazashvili, How do Fermi liquids get heavy and die? *J. Phys.: Condens. Matter* **13**, R723(R) (2001).
- [7] Q. Si, S. Rabello, K. Ingersent, and J. L. Smith, Locally critical quantum phase transitions in strongly correlated metals, *Nature (London)* **413**, 804 (2001).
- [8] M. Gulácsi, The one-dimensional Kondo lattice model at partial band filling, *Adv. Phys.* **53**, 769 (2004).
- [9] S. Lucas, K. Grube, C.-L. Huang, A. Sakai, S. Wunderlich, E. L. Green, J. Wosnitza, V. Fritsch, P. Gegenwart, O. Stockert, and H. von Löhneysen, Entropy evolution in the magnetic phases of partially frustrated CePdAl, *Phys. Rev. Lett.* **118**, 107204 (2017).
- [10] W. Xie, F. Du, X. Y. Zheng, H. Su, Z. Y. Nie, B. Q. Liu, Y. H. Xia, T. Shang, C. Cao, M. Smidman, T. Takabatake, and H. Q. Yuan, Semimetallic Kondo lattice behavior in YbPdAs with a distorted kagome structure, *Phys. Rev. B* **106**, 075132 (2022).
- [11] C. Kourris and M. Vojta, Kondo screening and coherence in kagome local-moment metals: Energy scales of heavy fermions in the presence of flat bands, *Phys. Rev. B* **108**, 235106 (2023).
- [12] P. Nozières and A. Blandin, Kondo effect in real metals, *J. Phys. France* **41**, 193 (1980).

- [13] A. M. Tsvelik and M. Reizer, Phenomenological theory of non-Fermi-liquid heavy-fermion alloys, *Phys. Rev. B* **48**, 9887 (1993).
- [14] P. Coleman, in *Handbook of Magnetism and Advanced Magnetic Materials*, edited by H. Kronmüller and S. Parkin (John Wiley & Sons, New York, 2007).
- [15] Y. Tokiwa, M. Garst, P. Gegenwart, S. L. Bud'ko, and P. C. Canfield, Quantum bicriticality in the heavy-fermion metamagnet YbAgGe, *Phys. Rev. Lett.* **111**, 116401 (2013).
- [16] V. Fritsch, N. Bagrets, G. Goll, W. Kittler, M. J. Wolf, K. Grube, and C.-L. Huang, and H. von Löhneysen, Approaching quantum criticality in a partially geometrically frustrated heavy-fermion metal, *Phys. Rev. B* **89**, 054416 (2014).
- [17] Y. Tokiwa, C. Stingl, M. S. Kim, T. Takabatake, and P. Gegenwart, Characteristic signatures of quantum criticality driven by geometrical frustration, *Sci. Adv.* **1**, e1500001 (2015).
- [18] W. Zhu and J.-X. Zhu, Local quantum criticality of a one-dimensional Kondo insulator model, *Phys. Rev. B* **97**, 245119 (2018).
- [19] J. Zhang, H. Zhao, M. Lv, S. Hu, Y. Isikawa, Y. Yang, Q. Si, F. Steglich, and P. Sun, Quantum-critical phase from frustrated magnetism in a strongly correlated metal, *Nat. Phys.* **15**, 1261 (2019).
- [20] S. Kittaka, Y. Kono, S. Tsuda, T. Takabatake, and T. Sakakibara, Field-angle-resolved landscape of non-Fermi-liquid behavior in the quasi-kagome Kondo lattice CeRhSn, *J. Phys. Soc. Jpn.* **90**, 064703 (2021).
- [21] J. Kondo, Resistance minimum in dilute magnetic alloys, *Prog. Theor. Phys.* **32**, 37 (1964).
- [22] H. Suhl, Dispersion theory of the Kondo effect, *Phys. Rev.* **138**, A515 (1965).
- [23] E. S. Sørensen and I. Affleck, Scaling theory of the Kondo screening cloud, *Phys. Rev. B* **53**, 9153 (1996).
- [24] M. Sigrist, H. Tsunetsuga, and K. Ueda, Rigorous results for the one-electron Kondo-lattice model, *Phys. Rev. Lett.* **67**, 2211 (1991).
- [25] M. Sigrist, H. Tsunetsuga, K. Ueda, and T. M. Rice, Ferromagnetism in the strong-coupling regime of the one-dimensional Kondo-lattice model, *Phys. Rev. B* **46**, 13838 (1992).
- [26] T. Yanagisawa and K. Harigaya, Ferromagnetic transition of the Kondo lattice with Coulomb repulsion: Exact results, *Phys. Rev. B* **50**, 9577 (1994).
- [27] M. Troyer and D. Würtz, Ferromagnetism of the one-dimensional Kondo-lattice model: A quantum Monte Carlo study, *Phys. Rev. B* **47**, 2886 (1993).
- [28] S. Moukouri and L. G. Caron, Ground-state properties of the one-dimensional Kondo lattice at partial band filling, *Phys. Rev. B* **52**, R15723 (1995).
- [29] I. P. McCulloch, A. Juozapavicius, A. Rosengren, and M. Gulácsi, Ferromagnetism in Kondo lattice models, *Philos. Mag. Lett.* **81**, 869 (2001).
- [30] I. P. McCulloch, A. Juozapavicius, A. Rosengren, and M. Gulácsi, Localized spin ordering in Kondo lattice models, *Phys. Rev. B* **65**, 052410 (2002).
- [31] S. A. Basylko, P. H. Lundow, and A. Rosengren, One-dimensional Kondo lattice model studied through numerical diagonalization, *Phys. Rev. B* **77**, 073103 (2008).
- [32] R. Peters and N. Kawakami, Ferromagnetic state in the one-dimensional Kondo lattice model, *Phys. Rev. B* **86**, 165107 (2012).
- [33] H. Tsunetsuga, Y. Hatsugai, K. Ueda, and M. Sigrist, Spin-liquid ground state of the half-filled Kondo lattice in one dimension, *Phys. Rev. B* **46**, 3175(R) (1992).
- [34] C. C. Yu and S. R. White, Numerical renormalization group study of the one-dimensional Kondo insulator, *Phys. Rev. Lett.* **71**, 3866 (1993).
- [35] N. Shibata, T. Nishino, K. Ueda, and C. Ishii, Spin and charge gaps in the one-dimensional Kondo-lattice model with Coulomb interaction between conduction electrons, *Phys. Rev. B* **53**, R8828(R) (1996).
- [36] E. Novais, E. Miranda, A. H. Castro Neto, and G. G. Cabrera, Phase diagram of the anisotropic Kondo chain, *Phys. Rev. Lett.* **88**, 217201 (2002).
- [37] M. Nakagawa and N. Kawakami, Laser-induced Kondo effect in ultracold alkaline-earth fermions, *Phys. Rev. Lett.* **115**, 165303 (2015).
- [38] R. Zhang, D. Zhang, Y. Cheng, W. Chen, P. Zhang, and H. Zhai, Kondo effect in alkaline-earth-metal atomic gases with confinement-induced resonances, *Phys. Rev. A* **93**, 043601 (2016).
- [39] T. A. Costi and C. Kieffer, Equilibrium dynamics of the dissipative two-state system, *Phys. Rev. Lett.* **76**, 1683 (1996).
- [40] T. A. Costi, Scaling and Universality in the anisotropic Kondo model and the dissipative two-state system, *Phys. Rev. Lett.* **80**, 1038 (1998).
- [41] M. Kanász-Nagy, Y. Ashida, T. Shi, C. P. Moca, T. N. Ikeda, S. Fölling, J. Ignacio Cirac, G. Zaránd, and Eugene A. Demler, Exploring the anisotropic Kondo model in and out of equilibrium with alkaline-earth atoms, *Phys. Rev. B* **97**, 155156 (2018).
- [42] H. Ishizuka and Y. Motome, Partial disorder in an Ising-spin Kondo lattice model on a triangular lattice, *Phys. Rev. Lett.* **108**, 257205 (2012).
- [43] H. Ishizuka and Y. Motome, Thermally induced phases in an Ising Kondo lattice model on a triangular lattice: Partial disorder and Kosterlitz-Thouless state, *Phys. Rev. B* **87**, 155156 (2013).
- [44] H. Ishizuka and Y. Motome, Loop liquid in an Ising-spin Kondo lattice model on a kagome lattice, *Phys. Rev. B* **88**, 081105(R) (2013).
- [45] H. Ishizuka and Y. Motome, Exotic magnetic phases in an Ising-spin Kondo lattice model on a kagome lattice, *Phys. Rev. B* **91**, 085110 (2015).
- [46] A. E. Sikkema, W. J. L. Buyers, I. Affleck, and J. Gan, Ising-Kondo lattice with transverse field: A possible f-moment Hamiltonian for URu<sub>2</sub>Si<sub>2</sub>, *Phys. Rev. B* **54**, 9322 (1996).
- [47] J. Shin, Z. Schlesinger, and B. S. Shastry, Kondo-Ising and tight-binding models for TmB<sub>4</sub>, *Phys. Rev. B* **95**, 205140 (2017).
- [48] S. Tsuda, C. L. Yang, Y. Shimura, K. Umeo, H. Fukuoka, Y. Yamane, T. Onimaru, T. Takabatake, N. Kikugawa, T. Terashima, H. T. Hirose, S. Uji, S. Kittaka, and T. Sakakibara, Metamagnetic crossover in the quasikagome Ising Kondo-lattice compound CeIrSn, *Phys. Rev. B* **98**, 155147 (2018).
- [49] B. Li, J.-Q. Yan, D. M. Pajerowski, E. Gordon, A.-M. Nedić, Y. Szyzuk, L. Ke, P. P. Orth, D. Vaknin, and R. J. McQueeney, Competing magnetic interactions in the antiferromagnetic topological insulator MnBi<sub>2</sub>Te<sub>4</sub>, *Phys. Rev. Lett.* **124**, 167204 (2020).



- [50] W.-W. Yang, J. Zhao, H.-G. Luo, and Y. Zhong, Exactly solvable Kondo lattice model in the anisotropic limit, *Phys. Rev. B* **100**, 045148 (2019).
- [51] W.-W. Yang, Y. Zhong, and H.-G. Luo, Hexagonal Ising-Kondo lattice: An implication for intrinsic antiferromagnetic topological insulator, *Phys. Rev. B* **102**, 195141 (2020).
- [52] W.-W. Yang, Y.-X. Li, Y. Zhong, and H.-G. Luo, Doping a Mott insulator in an Ising-Kondo lattice: Strange metal and Mott criticality, *Phys. Rev. B* **104**, 165146 (2021).
- [53] S. R. White, Density matrix formulation for quantum renormalization groups, *Phys. Rev. Lett.* **69**, 2863 (1992).
- [54] U. Schollwöck, The density-matrix renormalization group, *Rev. Mod. Phys.* **77**, 259 (2005).
- [55] E. Dagotto, S. Yunoki, A. L. Malvezzi, A. Moreo, J. Hu, S. Capponi, D. Poilblanc, and N. Furukawa, Ferromagnetic Kondo model for manganites: Phase diagram, charge segregation, and influence of quantum localized spins, *Phys. Rev. B* **58**, 6414 (1998).
- [56] D. J. Garcia, K. Hallberg, B. Alascio, and M. Avignon, Spin order in one-dimensional Kondo and Hund lattices, *Phys. Rev. Lett.* **93**, 177204 (2004).
- [57] E. Fradkin, *Field Theories of Condensed Matter Physics* (Cambridge University Press, Cambridge, 2013), 2nd ed., Chap. 3.
- [58] Y. Chen, Z. Yu, and H. Zhai, Superradiance of degenerate Fermi gases in a cavity, *Phys. Rev. Lett.* **112**, 143004 (2014).
- [59] R. Peierls, *Quantum Theory of Solids*, International Series of Monographs on Physics (Clarendon Press, Oxford, 1955).
- [60] A. Auerbach, *Interacting Electrons and Quantum Magnetism* (Springer-Verlag, New York, 1994).
- [61] Note that, essentially, the AIP considered in the IKL model is not a singlet since it has a doubly degenerate ground state, whereas a singlet is a unique non-degenerate state.
- [62] J. Eisert, M. Cramer, and M. B. Plenio, Area laws for the entanglement entropy, *Rev. Mod. Phys.* **82**, 277 (2010).
- [63] P. Calabrese and J. Cardy, Entanglement entropy and quantum field theory, *J. Stat. Mech. Theory Exp.* (2004) P06002.
- [64] A. Gaenko, A. Antipov, G. Carcassi, T. Chen, X. Chen, Q. Dong, L. Gamper, J. Gukelberger, R. Igarashi, S. Iskakov *et al.*, Updated core libraries of the ALPS project, *Comput. Phys. Commun.* **213**, 235 (2017).
- [65] B. Bauer, L. D. Carr, H. G. Evertz, A. Feiguin, J. Freire, S. Fuchs, L. Gamper, J. Gukelberger, E. Gull, S. Guertler, A. Hehn, R. Igarashi *et al.*, The ALPS project release 2.0: Open source software for strongly correlated systems, *J. Stat. Mech.: Theory Exp.* (2011) P05001.